Experimental and kinetic modeling study of NO formation in premixed CH_4+O_2+N_2 flames

Han, Xinlu; Marco, Lubrano Lavadera; Brackmann, Christian; Wang, Zhihua; He, Yong; Konnov, Alexander A.

Published in:
Combustion and Flame

DOI:
10.1016/j.combustflame.2020.10.010

2021

Document Version:
Publisher's PDF, also known as Version of record

Combustion and Flame 223 (2021) 349–360

Contents lists available at ScienceDirect

Combustion and Flame

journal homepage: www.elsevier.com/locate/combustflame

Experimental and kinetic modeling study of NO formation in premixed CH_4+O_2+N_2 flames

Xinlu Han[a,b,*], Marco Lubrano Lavadera[a], Christian Brackmann[a], Zhihua Wang[b], Yong He[b], Alexander A. Konnov[a]

[a] Division of Combustion Physics, Department of Physics, Lund University, Lund SE-22100, Sweden
[b] State Key Laboratory of Clean Energy Utilization, Zhejiang University, Hangzhou 310027, PR China

ARTICLE INFO

Article history:
Received 7 June 2020
Revised 6 October 2020
Accepted 7 October 2020
Available online 21 October 2020

Keywords:
Nitric oxide
Methane flame
Kinetic mechanism
Laminar burning velocity
LIF

ABSTRACT

The nitric oxide (NO) formation in methane (CH_4) flames has been widely investigated, with quite a few kinetic mechanisms available in the literature. However, studies have shown that there are often discrepancies between the simulations using various mechanisms and the experimental results. To elucidate reactions leading to these discrepancies, experiments were designed to measure the NO formation in the post flame zone of CH_4+O_2+N_2 flames with the oxygen ratio, $x_{O_2} = O_2/(O_2+N_2)$, varying from 0.2 to 0.27. The experiments were carried out on a heat flux burner at atmospheric pressure and 298 K using saturated Laser-induced fluorescence. The equivalence ratio, ϕ, was changed from 0.7 to 1.6. The corresponding laminar burning velocity, S_L, for each condition was also measured using the heat flux method. A comparison was made for the present experimental data and simulation results using the Konnov, Glarborg, NOMecha 2.0, and San Diego mechanisms, and none of them well reproduced the new NO experimental data for all investigated conditions. Numerical analyses show that the increment of NO mole fraction in stoichiometric and fuel-lean flames when the x_{O_2} increases is mostly defined by the thermal-NO production, which is found to be over-predicted, especially by the Konnov and San Diego mechanisms. The rate constant of reaction NO+N = N_2+O was derived as $k = 1.529 \times 10^{13} T^{-0.0027} \exp(\frac{185.41[cal/mole]}{RT})$ cm^3 / mol s over 225–2400 K temperature range. The rate constants of four reactions controlling CH mole fraction profiles and prompt-NO formation were updated based on the analysis of the literature data that yields an improved performance of the Konnov mechanism.

1. Introduction

Emission of nitric oxide (NO) from combustion processes has, for a long time, been an environmental concern, and the more and more stringent restrictions on NO emissions have driven thousands of researchers to investigate the underlying chemistry. Due to its dominance in natural gas and with the simplest chemical structure among hydrocarbon fuels, the NO formation in methane (CH_4) flames has been examined at various temperatures and pressures. Nowadays, reaction pathways through the thermal- and prompt-NO formation, as well as the routes involving N_2O, NNH, HCN, etc. have been revealed with lots of kinetic mechanisms available for simulation, e.g., [1–8]. However, developing a robust mechanism whose predictions uniformly agree with available experimental results from CH_4 flames is still an unfinished task.

In the recent work of Brackmann et al. [9], the NO mole fractions formed in atmospheric CH_4+air flames were measured using laser-induced fluorescence (LIF) and compared with simulations using several mechanisms: GRI mech 3.0 [3], San Diego [4], Konnov (2009) [2], NOMecha 2.0 [5], Glarborg et al. [1], and Shrestha et al. [6]; however, none of the six mechanisms tested could well predict NO mole fractions in the whole range of equivalence ratios covered from $\phi = 0.7$ to 1.5. Earlier experiments and simulations carried out using a similar setup by Zhou et al. [10], and Wang et al. [11] demonstrated that the CRECK [12], GDF-kin 3.0 [7], and Mendiara-Glarborg [8] mechanisms could not predict experimental data well either. Though for some of the above-mentioned mechanisms updated versions have been released with improvements in various aspects (e.g., Mendiara and Glarborg [8] is an early version of Glarborg et al. [1], and NOMecha 2.0 [5] originates from GDF-kin 3.0 [7]), their simulation results for methane flames are still

* Corresponding author at: Division of Combustion Physics, Department of Physics, Lund University, Lund SE-22100, Sweden.
E-mail addresses: hanxinlu@zju.edu.cn, itinomiya@sina.cn (X. Han).

https://doi.org/10.1016/j.combustflame.2020.10.010
0010-2180/

unsatisfactory. Various discrepancies can also be found in other investigations using different experimental setups, e.g., [13,14].

Differences between numerical and experimental results prove the need for further updating of the existing mechanisms, which is also necessary considering the large uncertainties that remain, especially in the reactions governing the NO formation. One example is the rate-limiting thermal NO reaction

$$N+NO=N_2+O. \quad (R1)$$

Though the rate constant of reaction (R1) has been widely investigated since the last century, e.g., [15–27], a scattering range of it spans over almost an order of magnitude as seen from the review of Baulch et al. [28]. Their recommendation for the rate constant of reaction (R1) was given with an uncertainty of a factor of 2 for the 210–3700 K temperature range. For the reverse reaction (R-1) in the temperature range 1700–4000 K, the uncertainty was estimated to be ± 40%. Abián et al. [29] noted the inconsistency of the evaluations for the forward and reverse rate constants from [28] and performed dedicated experiments on NO formation in a flow reactor. The error limits were then improved down to ± 30% for the reverse reaction (R-1) over the temperature range 1700–1800 K, while the recommended value for the rate constant of the forward reaction was given for the 250–3000 K range. Buczkó et al. [30] also used the experimental data of Abián et al. [29] to optimize the rate constants of reaction (R1) and reaction

$$N_2O+O=NO+NO. \quad (R2)$$

In the range 1600–2200 K, they derived a somewhat lower rate constant for (R1) and refined the uncertainty range compared to the evaluation of Baulch et al. [28]. Due to the high impact of (R1) on the thermal-NO formation, different rate parameters of this reaction lead to very different predictions of NO mole fractions in lean and stoichiometric CH_4 flames using various mechanisms [9].

Experimental studies of the NO formation in premixed flames are often used for model validation. However, simulations using detailed kinetic mechanisms are usually carried out based on idealized one-dimensional flame models, while real flames can be affected by non-idealities. For instance, in the early work of Konnov et al. [31], the axial and radial distributions of NO in atmospheric CH_4+air flames were measured using probe sampling, demonstrating that the radial profiles of NO are only flat in the core region of the moderately lean to moderately rich flames. In the very lean mixtures, at $\phi = 0.7$, the ambient air dilutes the burnt gases, and in the very rich mixtures at $\phi = 1.4$, oxidation of the combustion products occurs when sampling at a distance of 10 mm from the flame front. Thus, species diffusion to and from the environment could be influential for the NO measurements, which are then reasonable to be different from the simulation results. Another issue is the complex heat loss mechanism from the post-flame zone to the environment. The temperature profiles in atmospheric CH_4 flames stabilized on the heat flux burner have been measured by Bosschaart et al. using CARS thermometry [32] and also derived by van Maaren and de Goey from Laser Doppler Velocimetry measurements [33], where experimental results agree well with calculations considering the radiative heat losses. The uncertainty of the post-flame zone temperature can propagate to the uncertainty of the simulated NO mole fractions, which are quite sensitive to the post-flame zone heat losses [31]. To take these heat losses into account in the modeling using an earlier version of CHEMKIN-II, an imposed temperature gradient of −100 K/cm was suggested [31] based on the mentioned measurements [32,33] and used in similar studies, e.g., [10,11,33,34]. As can be expected, the above two issues are strongly coupled with the design of the testing system, and measurements at different positions of the flame should be influenced differently. Therefore, to make a more consistent comparison with the simulations, experiments at the less affected positions are needed, which cannot be performed using probes [31] but can be achieved by laser diagnostics to maintain high spatial resolution while being non-intrusive.

Based on the background outlined above, in the present work NO mole fractions and burning velocities of $CH_4 + O_2 + N_2$ flames having different oxygen contents x_{O_2} were measured. This design allows visiting as wide as possible range of experimental conditions and, what is more, increasing x_{O_2} makes the flame temperature change widely, which permits covering a region of parameter space where NO formation is increasingly sensitive to the thermal-NO reactions.

2. Experimental details

The experimental setup used herein is nearly the same as that in the previous study of Brackmann et al. [9] except that a burner of improved design [35] was used in the present experiments. This improved design allows the stabilization of faster-burning flames compared with the traditional heat flux burner, which helps investigate conditions with high oxygen content. All the experiments were conducted at atmospheric pressure and initial gas mixture temperature of 298 K. The O_2 content in the oxidizer, denoted as $x_{O_2} = O_2/(O_2+N_2)$, was changed from 0.2 to 0.27 with 0.01 increments. At each x_{O_2}, the equivalence ratio ϕ was varied from 0.7 to 1.6 with 0.1 increments. Unburnt mixture flow rates of the investigated CH_4+O_2+N_2 flames were controlled by three individual mass flow controllers (MFC). The adiabatic laminar burning velocity S_L was measured by the heat flux method with the burner plate temperature being set at 368 K using a thermostatic water bath. The uncertainty of the measured S_L was evaluated from the radial scattering of the burner plate temperature measured by 15 thermocouples and the uncertainties of the mass flow controllers. A detailed description of the analysis of the heat flux method uncertainties has been given by Alekseev et al. [36]. After the measurement of S_L, adiabatic flame conditions were achieved by setting the inlet gas velocity equal to S_L, and the NO mole fraction was measured using saturated laser-induced fluorescence by excitation of the $A^2\Sigma^+ \leftarrow X^2\Pi$ (0–0) band according to the procedure presented by Brackmann et al. [9]. The relative uncertainty of the measured NO mole fractions was previously evaluated as ±8.7% when considering errors caused by calibration, flame temperature, and gas composition (affecting quenching and rotational energy transfer) uncertainties [9]. The evaluation of NO mole fractions includes corrections for temperature and quenching and the uncertainty is estimated by comparing differences in corrected signals from $\phi = 0.7$ syngas, CH_4, CH_3OH, and $\phi = 0.5$ syngas flames seeded with NO [9]. A more detailed explanation of the LIF measurements and their uncertainty can also be found in the Supplemental Material. For both S_L and NO mole fraction results, the uncertainty of the corresponding equivalence ratio ϕ was estimated from the uncertainty of the CH_4, N_2, and O_2 mass flow controllers. All experimental data with associated uncertainties are tabulated in the Supplemental Material.

To assess uncertainties associated with the radiative heat loss modeling, the NO mole fraction was measured at 5 mm height above the burner plate (HAB). This position is only a little bit downstream of the flame front and thus, less affected by the heat loss to the environment in the post-flame zone than measurement points at higher HAB. Also, the NO results at $\phi > 1.5$ will not be compared with the simulations due to the following reasons. Figure 1 shows the NO experimental results for CH_4+air flames at HAB = 5 mm and 10 mm. Around stoichiometry, the NO mole fractions at 5 mm are lower than at 10 mm due to a shorter time for the formation of thermal NO. It is also found that the measured

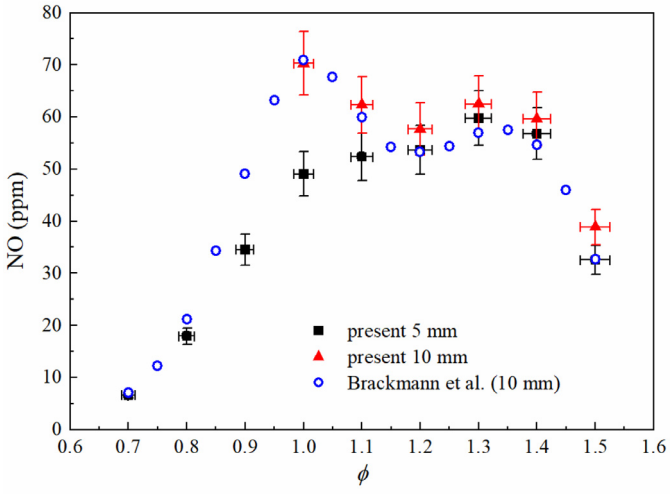

Fig. 1. NO mole fractions in CH_4+air flames measured at different HAB, at 1 atm and 298 K.

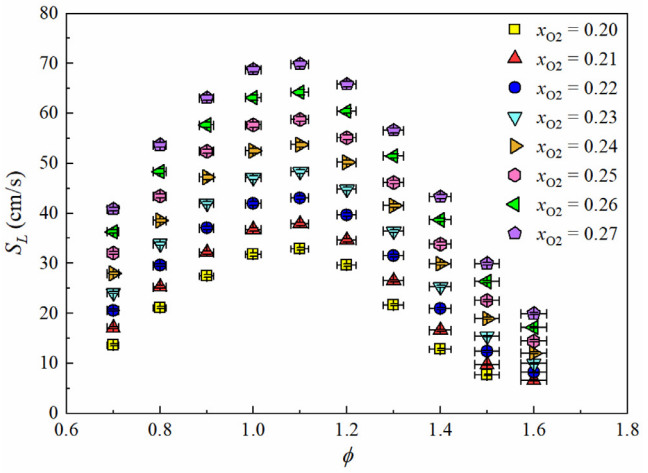

Fig. 2. Measured laminar burning velocity of CH_4+N_2+O_2 mixtures with different x_{O_2} versus ϕ, at 1 atm and 298 K.

NO mole fraction at $\phi = 1.5$ increases with HAB. However, in the very rich mixtures, the dominant prompt NO is formed inside the flame front and should not change with height. One reasonable explanation for this trend is that the real flame is not one-dimensional, and the NO formed by the outer conical diffusion flame layer diffuses into the measurement point at the center of the flame. At the lower height, the distance of transportation is longer, and the result is closer to the NO formed by the flame itself. This consideration agrees with the findings of Konnov et al. [31]. Therefore, a comparison of the experimental data and one-dimensional simulations at $\phi = 1.5$ is only made to indicate the possible impact of the flame non-idealities on the kinetic model validation. Data at $\phi < 1.5$ are considered to not be influenced by the flame non-idealities since the off-stoichiometric measurement results at different heights are close to each other and overlap within the uncertainty.

Figure 1 also shows the experimental data by Brackmann et al. [9] at HAB = 10 mm, compared with which the present experimental data are slightly higher at the fuel-rich side. Besides data scattering in the measurement, another reason for this discrepancy is that the usage of individual N_2 and O_2 MFCs rather than one air MFC in the present setup introduced extra uncertainties in the equivalence ratio and the oxidizer composition, which are shown as the error bars in Fig. 1. Nevertheless, it is found that the data from Brackmann et al. [9] are in agreement with the present measurements within the overlapping uncertainties.

3. Modeling details

Simulations were carried out using ANSYS CHEMKIN 17.0 [37] and kinetic mechanisms from San Diego [4], NOMecha2.0 [14], Glarborg [1], and Konnov [38] because they, or some early versions of them, were widely tested in NO-related combustion studies, e.g., [9]. Here the San Diego mechanism specifically refers to the combination of the 2016-12-14 main mechanism and the 2004-12-09 (2) nitrogen chemistry [4]. The NOMecha2.0 mechanism used herein was recently released by de Persis et al. [14] and validated for atmospheric and high-pressure flames; thus, it gives much better predictions against the laminar burning velocities investigated here than the earlier version [5] used in ref. [9].

During the calculations, the CURV and GRAD parameters were set at 0.02 and 0.05, respectively. Radiation heat losses were taken into account because they influence the simulated temperature profile and thus the NO mole fraction. The modeling of the radiation heat losses in ANSYS CHEMKIN is based on the assumption that the radiation is from an optically thin layer, and the radiation from CO, CO_2, CH_4, and H_2O was considered in the present study. It should be noted that among the four chosen mechanisms, only the Konnov mechanism includes the absorption coefficients of the radiative species, which are taken from the work of Nakamura and Shindo [39]. To make a fair comparison, the same coefficients were added to the Glarborg, San Diego, and NOMecha2.0 mechanisms, which originally do not include them. The NO mole fractions used to compare with the experimental results were selected at 5 mm downstream the calculated point where the temperature equals the burner plate temperature of 368 K.

4. Result and discussions

4.1. Burning velocity and NO mole fraction

Figure 2 shows the present experimental results of the laminar burning velocities at different x_{O_2}. The uncertainty of ϕ is shown as the error bars along the x-axis and increases with ϕ. The uncertainty of S_L, shown as the error bars along the y-axis is always less than 0.6 cm/s and thus hidden by the symbols in the plot. It is found that the S_L increases nearly linearly with x_{O_2}, and at around stoichiometry, the increment of S_L with $\Delta x_{O_2} = 0.01$ is ~5.5 cm/s. Data at $\phi = 1.6$, $x_{O_2} = 0.20$ were not measured since the flame was highly unstable.

Figure 3 shows the comparison between the experimental results and modeling of S_L using the four kinetic mechanisms, for x_{O_2}= 0.21 and 0.27. At x_{O_2}= 0.21, the results of the San Diego mechanism are slightly higher than the experimental data at the very lean side, and lower at the rich side. Results using NOMecha2.0 are slightly lower than the experimental results regardless of ϕ. Predictions of the Glarborg and Konnov mechanisms almost overlap and show better agreement with the experimental data than the San Diego and NOMecha 2.0 mechanisms. The tendencies of simulations at x_{O_2}= 0.27 are the same as at x_{O_2}= 0.21, with the differences among each other being more obvious due to the higher values of S_L.

Figure 4 shows the experimental results of NO mole fraction for different x_{O_2}. The measured NO mole fractions are found to increase with x_{O_2} at $\phi \leq 1.5$, indicating that both thermal and prompt NO formation is accelerated at higher oxygen content. Also, from x_{O_2}= 0.2 to 0.27, the equivalence ratio of the peak NO formation can be found to shift from $\phi = 1.3$ to $\phi = 1.0$, therefore, the

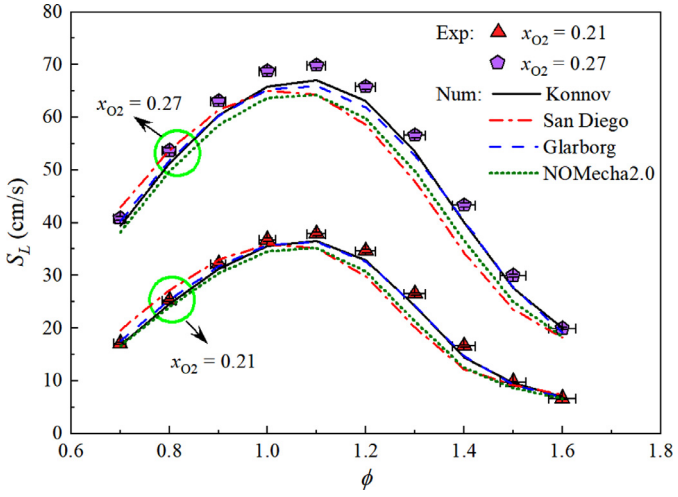

Fig. 3. Comparison of the experimental and simulated S_L for CH_4+N_2+O_2 mixtures with x_{O_2}= 0.21 and 0.27, at 1 atm and 298 K.

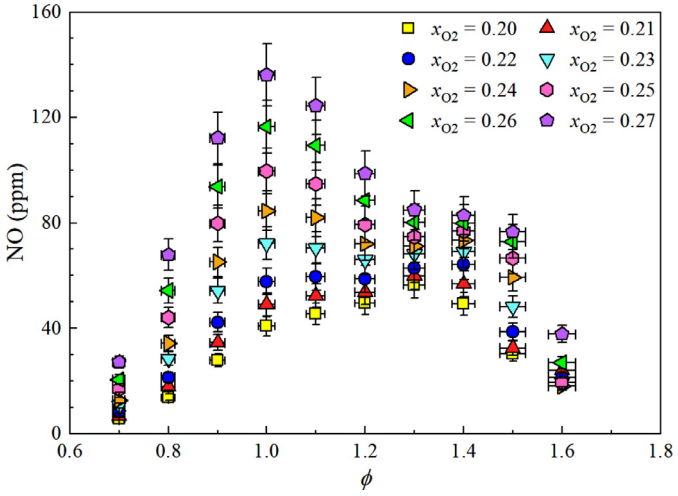

Fig. 4. Measured NO mole fraction in CH_4+N_2+O_2 flames at different oxygen ratios versus ϕ, at 1 atm and 298 K.

acceleration of the thermal NO production is more sensitive to x_{O_2} than that of the prompt NO. For the data at $\phi = 1.6$, an irregular sequence of the NO mole fractions at different x_{O_2} is noticed. Based on the radial distribution findings of Konnov et al. [31], the assumption can be made that the irregular sequence is caused by the competition of NO diffusion from the outer conical diffusion flame layer and convection increasing with S_L at different x_{O_2}, as has been discussed above. At $\phi = 1.5$, the contribution of these competing effects could also be present.

Figure 5 shows a comparison of the NO mole fractions obtained from measurements and simulations, for x_{O_2}= 0.21 and x_{O_2}= 0.27. At x_{O_2}= 0.21, the San Diego and Glarborg mechanisms underestimate while the Konnov mechanism over-estimates the experimental data. The NOMecha2.0 results agree well with the experimental data at $\phi < 1.3$, while being much lower at $\phi = 1.4$. At x_{O_2}= 0.27, numerical results of the San Diego and Konnov mechanisms are notably larger than the experimental data, especially at around stoichiometry; the discrepancies are higher than 50%. The NOMecha2.0 mechanism also overpredicts the experimental data, however, the largest discrepancy, 70%, is found at $\phi = 1.4$. Results using the Glarborg mechanism agree better with the experiments, while they are 17% lower at $\phi \geq 1.3$. Altogether, none of the four mechanisms can satisfactorily reproduce the cases investigated in

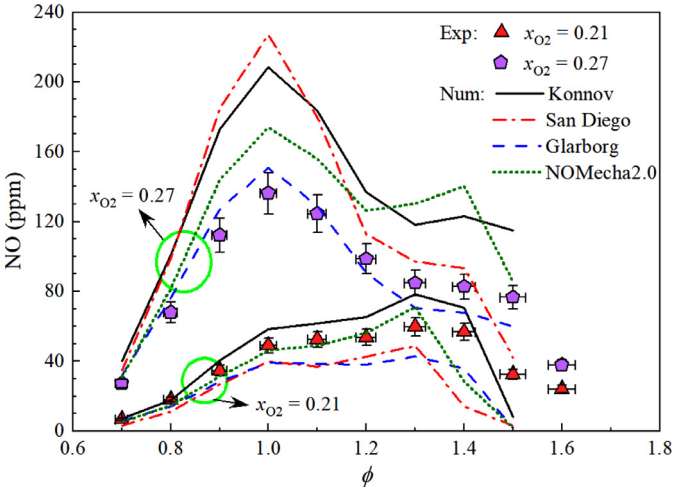

Fig. 5. Comparison of experimental and numerical NO mole fractions in CH_4+N_2+O_2 flames for x_{O_2} = 0.21 and 0.27, at 1 atm and 298 K.

the present study, even though some of them were shown to be the best among other kinetic mechanisms in predicting NO formation in the previous study [9].

4.2. Data analysis

4.2.1. Thermal NO

Different pathways of NO formation, such as thermal NO, prompt NO, N_2O, and NNH mechanisms, are operational in all flames of hydrocarbons, however, their contribution varies with the mixture composition. For instance, prompt NO is commonly accepted to be dominant in rich mixtures, while in near-stoichiometric flames, the thermal NO can be the major route if the reaction time is sufficient to produce NO. Comparing NO mole fractions formed at a fixed distance in different flames depicted in Fig. 4, one can see that the relative increase of [NO] with x_{O_2} in lean and stoichiometric mixtures is much higher than that in rich mixtures, which is certainly due to the largely different effective activation energies of the thermal- and prompt-NO formation. It can be assumed, therefore, that increment of the NO mole fraction between different flames of the same stoichiometry, but having different temperatures could be mostly defined by the thermal-NO mechanism.

Figure 6 shows the NO increment for stoichiometric flames, which was obtained by subtracting the NO mole fraction at $x_{O_2} = 0.2$ from the [NO] at higher x_{O_2} ($\Delta[NO]_{x_{O_2}} = [NO]_{x_{O_2}} - [NO]_{x_{O_2}=0.2}$). For the NO increment derived from the experiments, its uncertainty was evaluated as the root mean square of the NO uncertainties at x_{O_2} and $x_{O_2} = 0.2$. Also shown in Fig. 6 are the calculated NO increments using four kinetic mechanisms. Line 'Konnov (prompt NO removed)' presents the simulation results when all interaction reactions between C- and N- containing species in the Konnov mechanism have been manually deleted, which thus suppresses prompt-NO production. From the comparison between lines 'Konnov' and 'Konnov (prompt NO removed)' in Fig. 6, the prompt-NO production contributes less than 7% to the total NO increment. Therefore, the comparison of the NO increment and predictions of the four mechanisms assessed in Fig. 6 indicates that the thermal-NO production is overestimated by the models, especially by the Konnov and San Diego mechanisms, as also seen in Fig. 5, while the Glarborg model deviates from the experimental data only in high-temperature flames.

To examine which reactions lead to the difference between the experimentally and numerically derived NO incre-

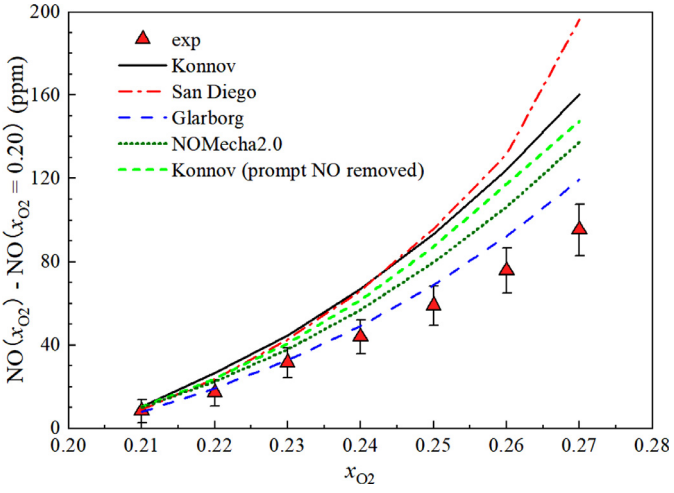

Fig. 6. Increment of the NO mole fraction versus x_{O_2} for stoichiometric $CH_4+N_2+O_2$ flames at 1 atm and 298 K.

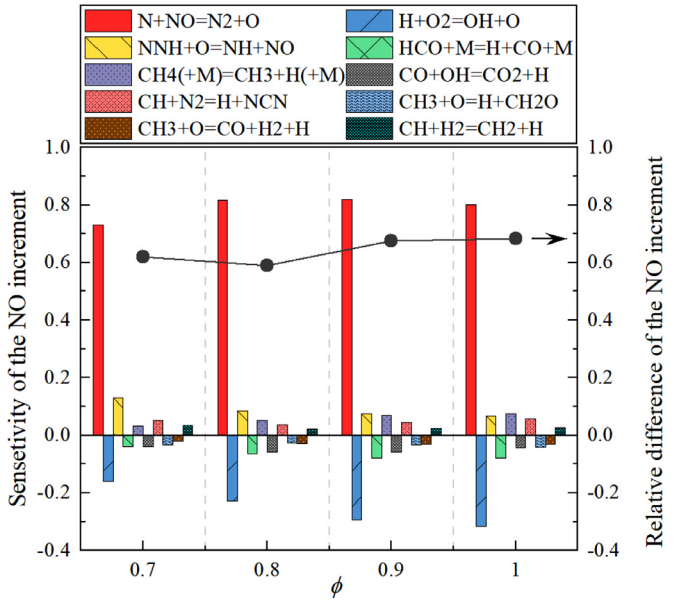

Fig. 7. Reaction sensitivity of the NO increment at $x_{O_2} = 0.27$ and the corresponding relative difference between the numerically and experimentally derived NO increment, for $\phi \leq 1$ $CH_4+N_2+O_2$ flames at 1 atm and 298 K.

ments, normalized A-factor reaction sensitivities of NO mole fraction were calculated using the Konnov mechanism. Sensitivities were calculated for the distance of 5 mm, $x_{O_2} = 0.2$ and 0.27, denoted $sens_{0.2}$ and $sens_{0.27}$, respectively. From these data, the sensitivity of the NO increment at $x_{O_2} = 0.27$ can be derived as $sens\Delta[NO]_{x_{O_2}=0.27} = (sens_{0.27} \cdot [NO]_{x_{O_2}=0.27} - sens_{0.2} \cdot [NO]_{x_{O_2}=0.2}) / \Delta[NO]_{x_{O_2}=0.27}$. Figure 7 shows the ten most sensitive reactions of the NO increment at $x_{O_2} = 0.27$, for lean and stoichiometric flames. The corresponding relative difference of the calculated NO increment using the Konnov mechanism compared with the experimental data is shown along the right y-axis of the same scale. From Fig. 7, reaction (R1) has the largest absolute sensitivity. Most of the other reactions are too important for the overall oxidation process and possess large sensitivity for the laminar burning velocity that should not be modified, for instance

Reactions

$$H + O_2 = OH + O. \quad (R3)$$

$$CH + N_2 = H + NCN \quad (R4)$$

$$NNH + O = NH + NO \quad (R5)$$

have positive sensitivities, which are several times lower than the relative difference between the numerically and experimentally derived NO increment, indicating that even turning their reaction rates to zero, the difference still cannot be compensated. Therefore, reaction (R1) is the only candidate for a modification that can improve the performance of the models. It should also be noted that the relative difference of the calculated NO increment (Fig. 7) is uniform in lean and stoichiometric flames; thus, all measurements in these flames can be implemented to derive the rate constant of reaction (R1).

The procedure of obtaining the rate constant using the experimentally determined increment of NO in different flames of the same stoichiometry essentially assumes that contributions of other mechanisms forming NO are subtracted and become negligible. This is not fully correct since the sensitivity of $\Delta[NO]_{x_{O_2}=0.27}$ to reaction (R1) is not unity, and the prompt-NO reactions contribute to the difference, as seen in Fig. 6. To avoid ambiguity, two models, namely the Konnov and Glarborg mechanisms, were used for analysis. These two models contain significantly different background chemistries since their selections of rate parameters for many reactions, which are sensitive to the NO predictions, are largely different. As a result, these two models show notably different behavior as seen in Fig. 6, and Fig. 5 clearly indicates that the prompt NO in rich methane flames is over-predicted by the Konnov and under-predicted by the Glarborg mechanisms. Thus, if the residual contribution of the prompt NO, NNH, and N_2O reaction routes affects the rate constant of reaction (R1) derived from the experimentally determined increment of NO, this would be manifested as specific trends different for these two models.

The procedure of the rate-constant determination was as follows. First, for all lean and stoichiometric flames shown in Fig. 4 at each equivalence ratio, the NO increments were obtained by subtracting the NO mole fraction at $x_{O_2} = 0.2$ from the [NO] at higher x_{O_2} ($\Delta[NO]_{x_{O_2}} = [NO]_{x_{O_2}} - [NO]_{x_{O_2}=0.2}$). The structure of each pair of the flames was then calculated using several (usually 3–5) fixed-rate constants of reaction (R1) in the range 1.0×10^{13} to 3.0×10^{13} $cm^3/mol\ s$. Using fixed values of the rate constant is substantiated by the fact that this reaction has very weak temperature dependence at high temperatures, as suggested and discussed in the earlier studies [17,18,20,21]. Values of $\Delta[NO]_{x_{O_2}}$ were then calculated in the same way as for the experimental data. These $\Delta[NO]_{x_{O_2}}$ for each rate constant showed linear variation with its value thus yielding brute-force sensitivity, which was found very close for the flames with $x_{O_2} = 0.2$ and $x_{O_2} = 0.27$ to the sensitivities shown in Fig. 7. The dependence $\Delta[NO]_{x_{O_2}}(k)$ confronted to the experimental data gives the optimum rate constant which was attributed to the temperature of the hotter flame, while the experimental uncertainty of the $\Delta[NO]_{x_{O_2}}$ is converted into the uncertainty of this rate constant using the brute-force sensitivity. Note, that for some flames having close temperature, e.g., with $x_{O_2} = 0.2$ and 0.21, the error bars of [NO] overlap (see Fig. 4), which produces unphysical negative lower limiting values of the rate constant. This procedure has been repeated using the two models, and results are shown in Fig. 8(a) with different symbols. The rate constants derived using the Glarborg model are systematically higher than those based on the Konnov model, however, the difference at higher temperatures, where the uncertainties are minimal, is typically within 20%. This minor difference indicates that the obtained reaction rates of (R1) are not influenced by choice of the kinetic

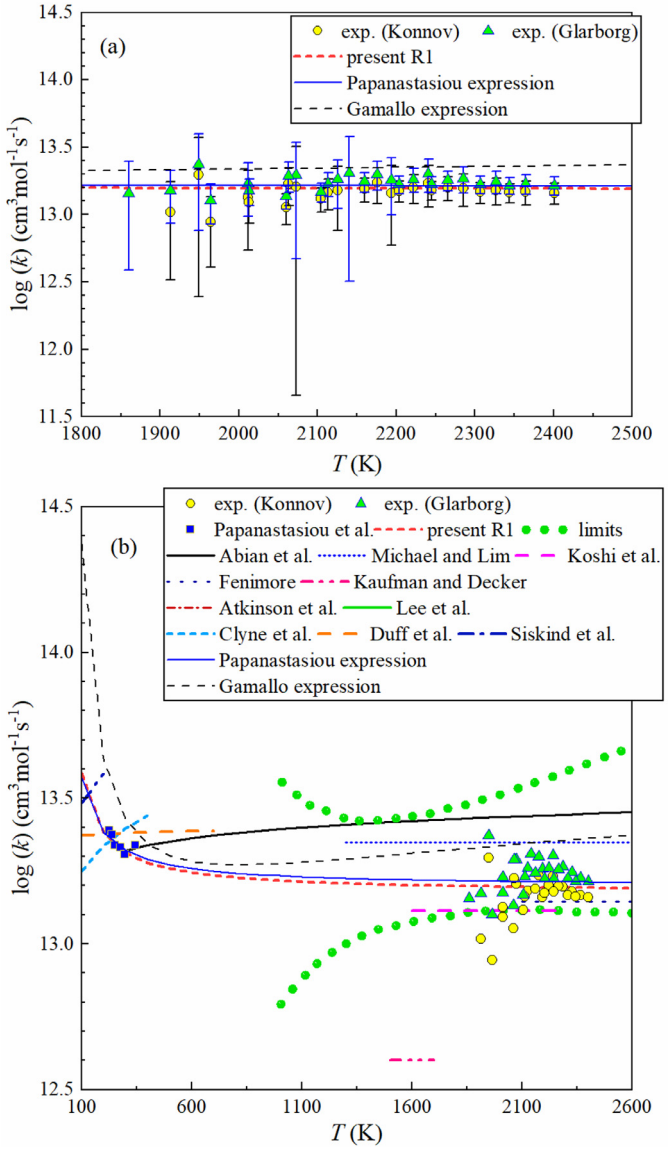

Fig. 8. Rate constants of R1 (NO+N = N_2+O) obtained using the experimental $\Delta[NO]_{x_{O_2}}$ data and two mechanisms (Panel (a)), and their comparison with the literature rate data (Panel (b)).

model implemented and thus by the residual contribution of the prompt-NO, NNH, and N_2O reactions.

The reaction rates obtained from the above procedure using both models were processed to fit the rate expression of (R1). To extend the expression to the low-temperature region, the recent high-precision experimental data by Papanastasiou et al. [40] from 225 to 344 K were included in the fitting process. Measurements by Papanastasiou et al. [40] were carried out using a discharge flow reactor coupled with resonance fluorescence detecting the O(3P) atoms, where reaction rate uncertainties less than 5% were reported. Their dataset is in excellent agreement with the measurements of Wennberg et al. [41] and Nakayama et al. [42] and within a 2σ uncertainty of the NASA/JPL [43] recommendation.

The non-linear fitting expression $k = 1.529 \times 10^{13} T^{-0.0027} \exp(\frac{185.41[cal/mole]}{RT})$ was achieved using the 'Generalized Nonlinear Non-analytic Chi-Square Fitting' code by Brahms [44] over the 225–2400 K temperature range. Uncertainties of the fitting parameters were also obtained from the code via propagation of the uncertainties in the experimental rate data and shown to be asymmetric as (+0, −45%) and (+36%, −45%) for the pre-exponential factor and the activation energy, respectively. It should be noted that experimental uncertainty of the NO measurements by LIF has very small impact on the derived rate constant and its uncertainties as illustrated in Fig. S8 in the Supplemental Material. Fig. 8 shows the fitting result as 'present R1', while Fig. 8(b) also presents the recently evaluated upper and lower uncertainty limits from Buczkó et al. [30] determined in the high-temperature region. Literature rate constants from Michael and Lim [17], Koshi et al. [18], Heberling [19], Fenimore [20], Kaufman and Decker [21], Bachmaier et al. [22], Atkinson et al. [23], Lee et al. [24], Clyne and McDermid [25], Duff and Sharma [26], and Siskind and Rusch [27] are shown for comparison. The same rate constants as in Fig. 8(b) are presented in Arrhenius coordinates in Fig. S9 in the Supplemental Material. Remarkably, the rate constant expression suggested by Papanastasiou et al. [40] for the 225–344 K temperature range and extrapolated to the flame temperatures is almost indistinguishable from the present rate data, see Fig. 8(a). Also notable is that the theoretical calculations of the rate constant (R1) by Gamallo et al. [45] are only slightly above the low-temperature [40] and the present data. Figure S10 in the Supplemental Material repeats the simulations shown in Fig. 6 after implementing the present R1 expression in the four mechanisms, where notable improvements are observed for all the mechanisms, but the extent varies. Besides the Konnov mechanism, the modified NOMecha 2.0 predictions also show good agreement with the experimentally determined NO increment, while the modified Glarborg and San Diego predictions decrease to the lower limit defined by the experimental uncertainty. The different extents of the changes in model predictions are attributed to the different background chemistries in these mechanisms leading to different sensitivity to R1.

The original (R1) rate constant in the Konnov mechanism is from Abián et al. [29], and was derived using experimental results on NO formation from N_2+O_2 mixtures in a flow reactor within the 1700–1800 K temperature range. The rate constant obtained in the present work is significantly lower at these temperatures, as seen in Fig. 8(b); it is, therefore, interesting to check the impact of the new rate expressions on the model performance at the conditions of the flow reactor experiments. Figure 9 shows the comparison of the simulated NO mole fractions in different N_2+O_2 mixtures with the experimental data by Abián et al. [29]. The present rate constant (R1) yields calculated NO mole fractions all lower than those using the original Konnov mechanism, however, most of them are within the experimental uncertainty. Moreover, the updated model behavior is actually very close to the predictions of the optimized mechanism suggested by Buczkó et al., and similar to the performance of several literature models tested therein [30]. One should note that calculated NO mole fractions at the conditions of the flow reactor experiments [29] are also controlled by the rate constant of reaction (R2) for which the optimized rate constant [30] is higher by a factor of 2–2.5 than the one adopted in the Konnov mechanism. To check the reverse reaction (R-1), its reaction rates were calculated from the present R1 expression and compared with the literature reaction rates by Baulch et al. [28] and Abián et al. [29]. Figure S11 shows that the present (R-1) has reaction rates lower than the literature data by 40–50%, which is within the claimed uncertainties [28,29]. The rate constants of all reactions discussed in the present work are listed in Table 1.

4.2.2. Prompt NO

The Konnov mechanism notably over predicted prompt-NO formation as clearly seen in rich flames (cf. Fig. 5). Systematic efforts of many groups focusing on the relevant flame chemistry,

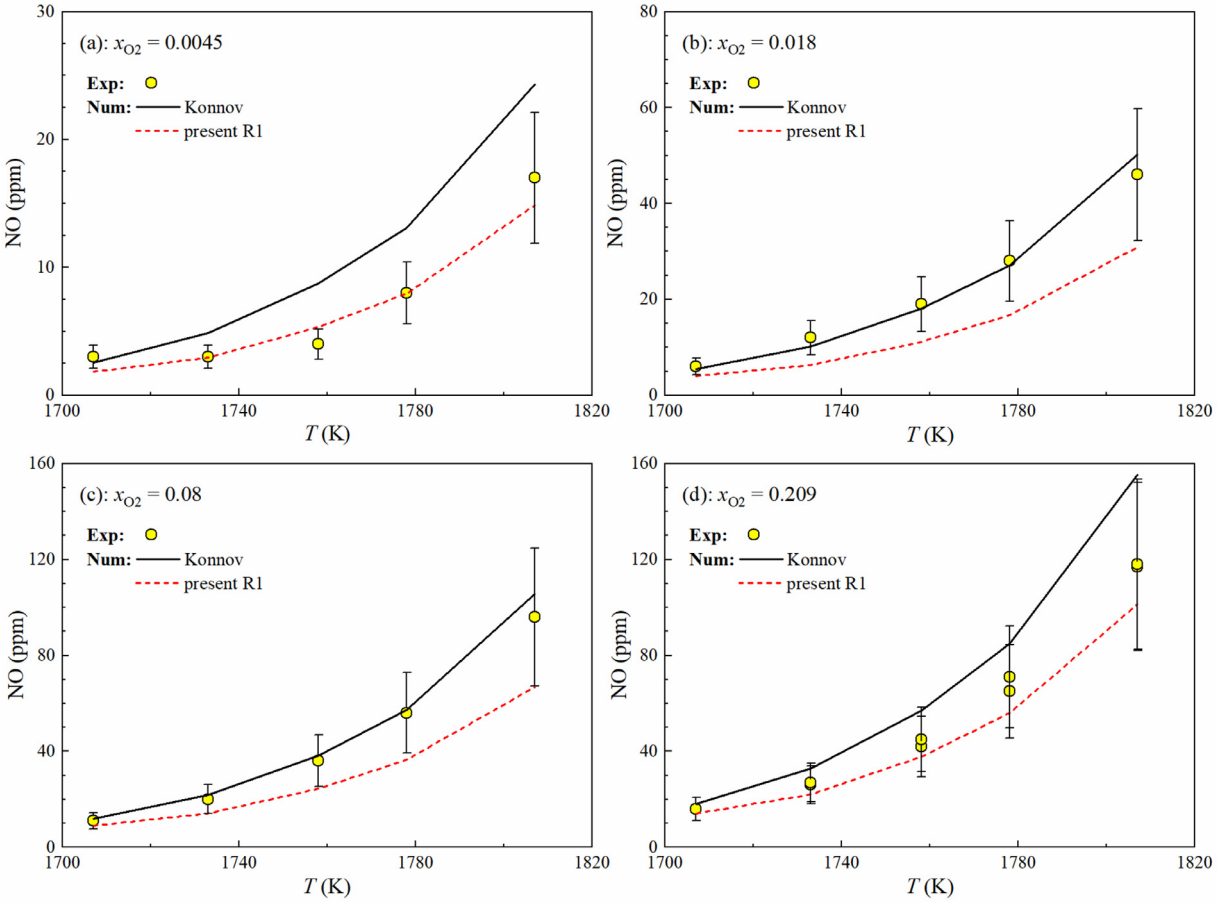

Fig. 9. Comparison of the simulated (lines) and experimental data [29] (symbols) for NO formation in N_2+O_2 mixtures.

Table 1
Selected reactions discussed in the present work. Units are s, mol, cm, cal in $k = AT^n \exp(-\frac{Ea}{RT})$, UF – uncertainty factor.

No.	Reaction	A	n	E_a	T range, K	UF	Ref.
R1	NO+N = N_2+O	1.53E+13	−0.0027	−185.41	225–2400	+0 −45%	p.w.
R2	N_2O+O=NO+NO	9.15E+13	0	27,680	1370–4080	1.6	[46]
R3	H + O_2=OH+O	1.04E+14	0	15,286.0	1100–3370	1.1	[47]
R4	CH+N_2=H+NCN	1.95E+12	0	16,915	800–1800	1.5	[7]
R5	NNH+O=NH+NO	2.00E+14	0	4000.0	1200–2500	2	[48]
R6	CH_2+N_2=HCN+NH	1.0E+13	0	74,000			[49]
R7	CH+H_2O=CH2O+H	2.8E+07	1.59	−2610	300–3000	2	[1]
R8	CH_2+H =CH+H_2	1.81E+14	0	60	220–1000	2	[50]
R9	CH+O_2=HCO+O	4.8E+12	0	0	290–800	2	[51]
R10	CH+O_2=H+CO+O	7.2E+12	0	0	290–800	2	[51]
R11	CH+O_2=CO_2+H	7.2E+12	0	0	290–800	2	[51]
R12	CH+O_2=CO+OH	4.8E+12	0	0	290–800	2	[51]
R13	CH+O_2=CO+OH*	3.24E+14	−0.4	4150	1200–2200	5	[52]

e.g., [5,14,53] allow for revisiting this sub-mechanism, while the present experimental data obtained over an extended range of flame temperatures are valuable validation targets. The prompt-NO formation is mostly controlled by the interaction between N_2 and CH, CH_2, $^1CH_2$ (singlet methylene) radicals, and it is, therefore, an integral characteristic defined by the rate constants of the key reactions (R4) and

$$CH_2+N_2=HCN+NH \quad (R6)$$

and by the mole fraction profiles of these radicals, mainly CH, as was emphasized in early studies, e.g., [7,54]. It is thus important to check model predictions of the radical profiles before modifying the rate constants of reactions (R4) and/or (R6).

In the work of Fomin et al. [51], the profiles of $^1CH_2$ have been measured in low-pressure CH_4+N_2+O_2 flames, and 78 rate constants of reactions along the pathway $CH_3 \rightarrow {}^1CH_2 \rightarrow CH_2 \rightarrow CH$ have been reviewed and updated in the Konnov mechanism. However, profiles of the CH radical, at the end of this pathway, have rarely been checked in CH_4 flames [5] using the previous version of the Konnov (2009) [2] mechanism only.

Most often the CH mole fraction profiles were measured in low-pressure burner-stabilized flames, e.g., by Thoman and McIlroy [55], Lamoureux et al. [5], and Berg et al. [56], while the data

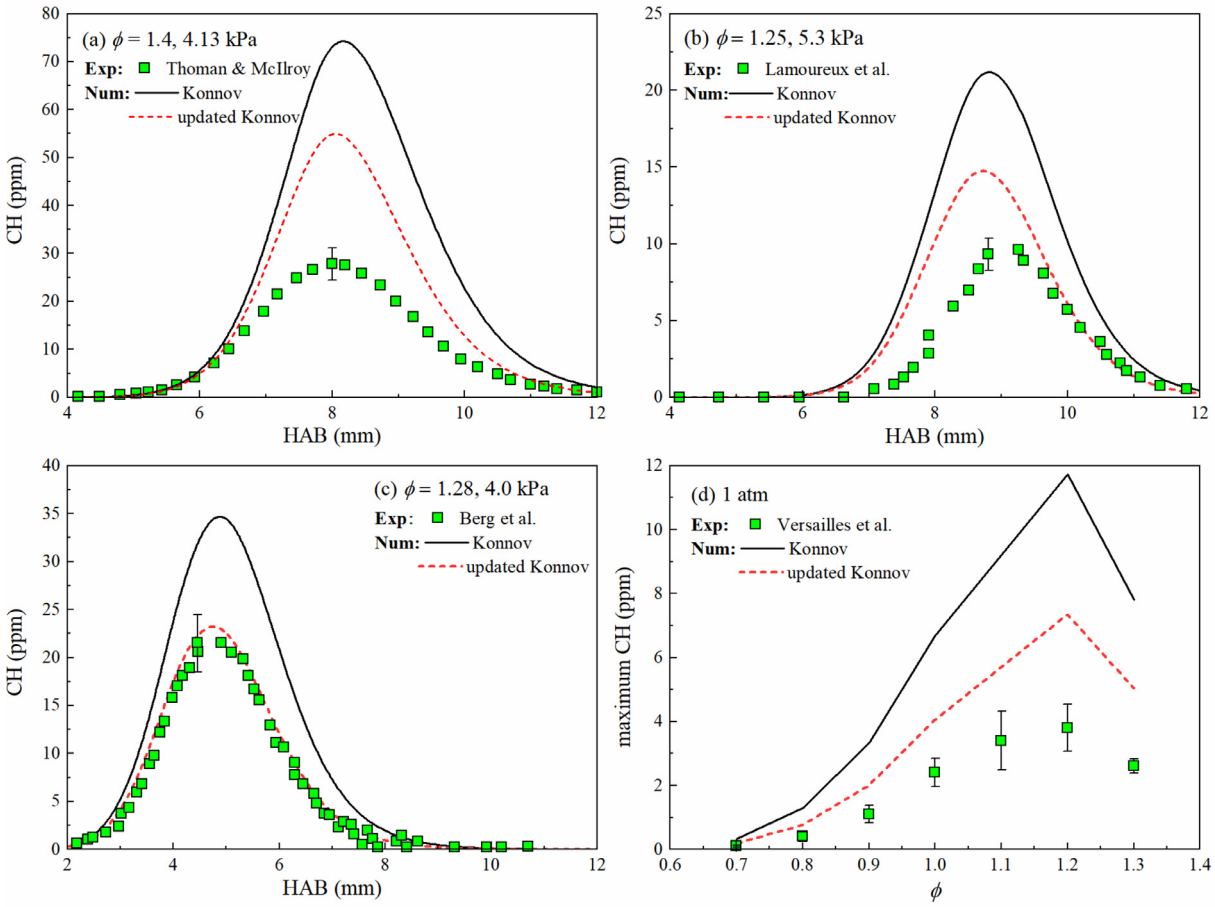

Fig. 10. Comparison of the simulated CH mole fractions in CH_4 flames with the experimental data of (a) Thoman and McIlroy [55], (b) Lamoureux et al. [5], (c) Berg et al. [56], and (d) Versailles et al. [57].

at atmospheric pressure are rather limited, for instance by Versailles et al. [57] obtained using stagnation flames, and by Evertsen et al. [58] on the heat flux burner. In the latter studies, only maximum CH mole fractions at different equivalence ratios were reported. Other experiments, summarized in [57], were performed in flame configurations that are challenging to compare with one-dimensional modeling.

Figure 10 shows the comparison of the simulated CH mole fractions in CH_4 flames using the latest Konnov [38] mechanism with selected experimental data in rich CH_4 flames. Other examples of assessment are provided in the Supplemental Material. In all cases, the mechanism significantly over-predicts the CH mole fractions that calls for revision of the rate constants controlling CH formation and consumption.

Sensitivity and reaction pathway analyses of CH formation and consumption for the flame conditions depicted in Fig. 10 and Figs. S12–S15 have been performed using the Konnov mechanism. The outcome of these analyses was very similar to that presented by Versailles et al. [57], who tested several kinetic models from the literature and is, for the sake of brevity, only shortly outlined here. Several reactions possess high sensitivity and control CH mole fractions in flames:

$$CH+H_2O=CH_2O+H \quad (R7)$$

$$CH_2+H=CH+H_2 \quad (R8)$$

$$CH+O_2=HCO+O \quad (R9)$$

Other reactions forming CH radicals from CH_2 in reactions with OH or consuming in reactions with O, OH, H, and CO_2 often share the same or very close rate constants in different models and have much lower sensitivities compared to reactions (R7)–(R9) [57]. The rate constant of (R7) adopted in the Konnov mechanism was from Bergeat et al. [59], who experimentally demonstrated that the product branching ratio of H-atom formation is 100% and performed ab initio calculations of k_7 over the range 100–700 K. In the Glarborg [1] and recent prompt-NO [53] mechanisms, new theoretical calculations made by Klippenstein up to 3000 K are implemented. The new rate constant of (R7) is in good agreement with the previous expression [59] at lower temperatures, yet has a minimum around 800 K and notably increases toward 2000 K, which affects calculated CH profiles.

Reaction (R8) has been investigated both in the forward and reverse directions with a smaller spread of data in the reverse one. Therefore, in the Konnov mechanism, the rate constant suggested by Baulch et al. [28] was adopted for reverse reaction (R-8). This recommendation was mostly based on the experimental data of Brownsword et al. [60] and of Becker et al. [61] at temperatures below 744 K. Earlier measurements of Zabarnick et al. [62] are found to be approximately two times lower than these studies, and indicate the room for the rate constant variation. Since then, no experimental studies of this reaction were attempted. In the present work, the rate constant of (R8) calculated by Garcia et al. [50] is adopted. The rate constant of the reverse reaction (R-8) calculated using thermodynamic data then agrees better with the measurements of Zabarnick et al. [62].

The reaction between CH and O_2 in the Konnov mechanism includes (R9) and other product channels:

$$CH+O_2=H+CO+O \quad (R10)$$

$$CH+O_2=CO_2+H \quad (R11)$$

$$CH+O_2=CO+OH \quad (R12)$$

$$CH+O_2=CO+OH^*. \quad (R13)$$

The total rate constant suggested by Baulch et al. [28] was adopted for reactions (R9)–(R12) together with the branching ratio obtained from the flow reactor experiments at 290 K–800 K by Bergeat et al. [63]. The second recommendation [28], provided for the range 2200–3500 K, is more than 3 times higher and was based on the experimental data of Röhrig et al. [64] and Markus et al. [65]. In some models, e.g., FFCM-1 [66] these two evaluations from Baulch et al. [28] were approximated by a fit yielding a rapidly increasing rate constant at high temperatures, which contradicts the theoretical studies [67,68] that predicted no or negative temperature dependence for the total rate. In the Glarborg [1] mechanism, only channels (R9) and (R10) are included with the rate constant of Röhrig et al. [64] and a theoretical rate constant accounting for prompt dissociation of HCO [69], respectively. The theoretical study of Keshavarz and Mousavipour [68] did not help to resolve the contradiction between low-temperature and high-temperature measurements since it did not consider product channels (R10) and (R13). The latter reaction has positive activation energy as was derived by Hall and Petersen [52] by fitting chemiluminescence profiles from shock tube experiments over the temperature range 1200–2200 K. However, their rate constant is more than an order of magnitude lower compared with the rates determined by Röhrig et al. [64] and Markus et al. [65]. On the other hand, the rate constant of (R13) derived at higher temperatures [52] does not agree with the low-temperature measurements of Carl et al. [70] in the 296–511 K range. Due to the controversies outlined above, the rate constants of reactions (R9)–(R12) have not been modified in the present work.

Nevertheless, updated rate constants of (R7) and (R8) bring a much better agreement with the CH measurements in CH_4 flames, as shown in Fig. 10 and Figs. S12–S15 in the Supplemental Material. Now that the model can better reproduce CH mole fraction profiles, the key prompt-NO reactions could be revisited. Recent dedicated models [5,14,53] suggested different modifications mostly centered around NCN chemistry. In the present work, only reactions (R4) and (R6) were inspected. For (R6), the rate constant from Miller and Bowman [49] was implemented to substitute the original expression of Sanders et al. [71] in the Konnov mechanism, since Miller and Bowman [49] pointed out that the assumption of the four-centered transition state [71] is questionable. This change significantly suppresses the role of CH_2 radicals in the prompt-NO formation, leaving reaction (R4) as the major player. The rate constant of (R4) in the Konnov mechanism of 2009 [2] was $k = 3 \times 10^{12} \exp(-\frac{221.57}{RT})$, which is half the value obtained from the shock tube measurements of Vasudevan et al. [72] at temperatures above 1943 K. In the recent models [5,14,53] the expressions implemented are significantly higher and very close to each other at temperatures above 1000 K. In the present updated mechanism the rate constant from Lamoureux et al. [7] was tested.

Modifications of the rate constants of (R4) and (R6)–(R8) do not significantly affect the calculated mole fraction profiles of NCN and HCN. The experimental data from Lamoureux et al. (NCN data from [73] and HCN data from [74]) in a low-pressure rich, $\phi = 1.25$, CH_4+ O_2 +N_2 flame were compared with the predictions of the original and modified mechanisms. The changes implemented slightly increase the maximum HCN and NCN mole fraction, which agrees worse with the experimental data of Lamoureux et al. [73,74] than the original Konnov mechanism, however, the latter is still within the experimental uncertainty, as illustrated in Fig. S16 in the Supplemental Material.

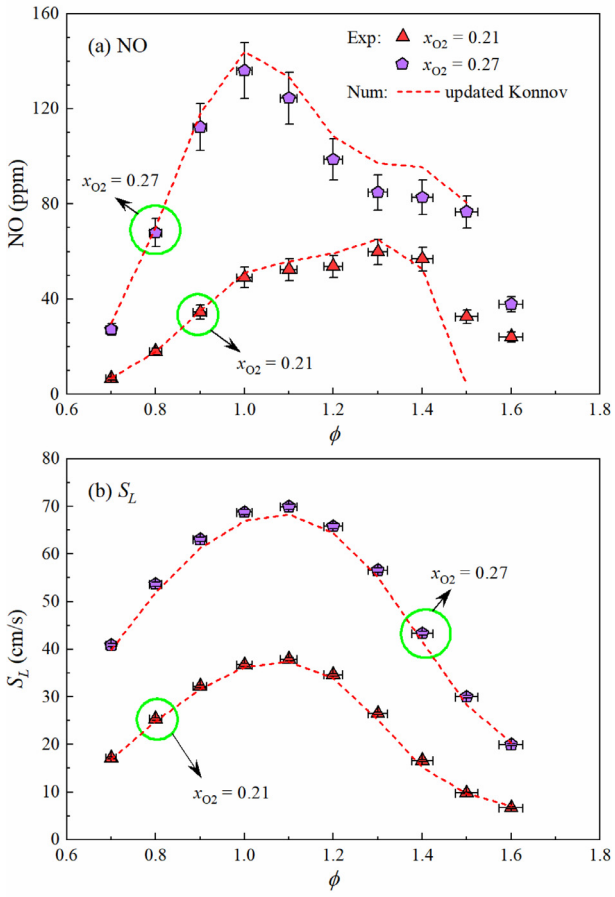

Fig. 11.. Comparison of the experimental results of NO mole fraction and laminar burning velocity in CH_4+O_2+N_2 flames with predictions of the updated mechanism.

New rate constants of (R1), (R4), and (R6)–(R8) significantly improve the performance of the Konnov mechanism. Figure 11 shows that the predictions using the updated model agree well with the present experimental data for the laminar burning velocity and NO mole fractions in that they are within the experimental uncertainties for most data points. Datasets at x_{O_2} = 0.21 and 0.27 are shown for the clarity of presentation, however, simulations at other oxygen contents also agree quite well with experimental data, as shown in Figs. S17 and S18 in the Supplemental Material. Comparing with the performance of the original model shown in Figs. 3 and 5, obvious improvement is achieved for the currently updated mechanism, that allows for analysis of the NO formation routes in the studied flames.

4.3. NO formation analysis

Figure 12 shows the reaction pathways from N_2 to NO for the investigated flames at x_{O_2}= 0.21 and 0.27, and ϕ = 1.0 and 1.4, which were computed using the currently updated Konnov mechanism. The thickness of the arrows in Fig. 12 represents the integrated rate of species production at HAB from 0 to 5 mm from a chemical step or a set of chemical steps normalized by that of reaction H + O_2 = OH + O (R3) at each condition. Besides, all reactions with a normalized rate of species production larger than

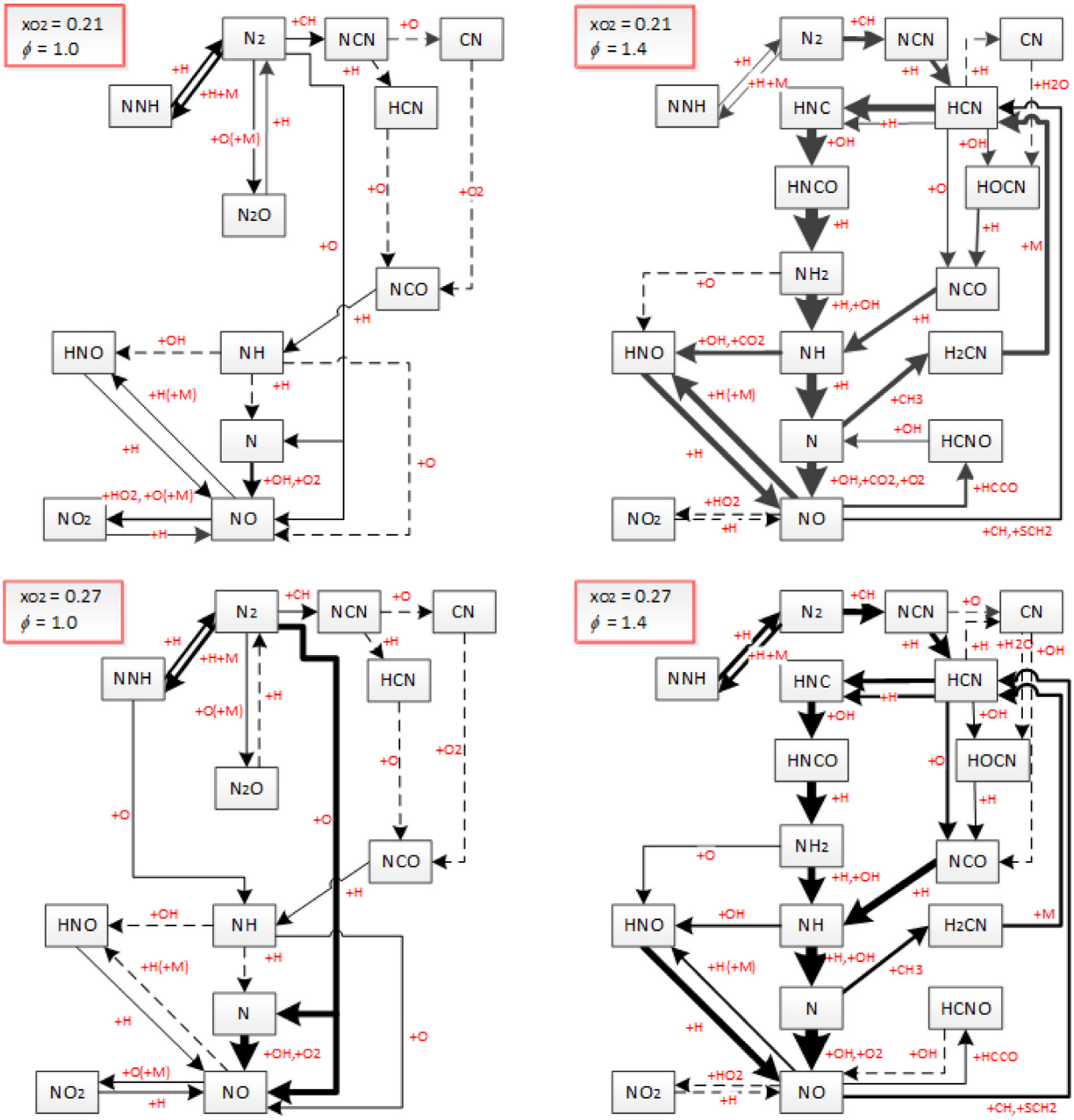

Fig. 12. NO formation pathways in CH_4+O_2+N_2 flames at x_{O_2}= 0.21 (top) and 0.27 (bottom); ϕ = 1.0 (left) and 1.4 (right).

5×10^{-5} are represented by solid lines, while the dashed lines denote some important reactions with a slightly lower rate of production. Reaction (R3) is the dominant reaction of producing OH and O radicals, and their rate of production is roughly proportional to the S_L, thus the normalization by (R3) excludes the influence of different S_L when comparing each combination of the oxygen contents and equivalence ratio. From Fig. 12, the difference of NO formation in ϕ = 1.0 and 1.4 flames can be clearly observed. At ϕ = 1.0, NO is formed mostly from (R1) and from reactions of N with OH and O_2, where the N atoms are produced mostly from (R1), too. At ϕ = 1.4, (R1) is no longer important, and the dominant route is $N_2 \rightarrow NCN \rightarrow HCN \rightarrow HNC \rightarrow HNCO \rightarrow NH_2 \rightarrow NH \rightarrow N \rightarrow NO$. The comparison of the reaction pathways at x_{O_2}= 0.21 and 0.27 shows that the increase of NO at higher x_{O_2} observed in the present study (see Fig. 3) at ϕ = 1.0 is defined by the increased rate of production via (R1), while the increase of the overall reactivity, manifested by the increase of S_L (see Fig. 2), is also influential. However, at ϕ = 1.4 the calculated reaction pathways are nearly the same for the flames with x_{O_2}= 0.21 and 0.27, therefore, the observed NO increase for higher x_{O_2} should mostly be attributed to the increase of the overall reactivity, which is mostly defined by the key chain-branching reaction (R3).

5. Conclusions

The present work was motivated by the discrepancies between modeling and experimental results of NO mole fractions in CH_4 flames. In the present experiments, NO measurements were carried out using laser-induced fluorescence in atmospheric CH_4+ O_2 +N_2 flames stabilized on a heat flux burner. The flame conditions were extended as much as possible, covering O_2 content x_{O_2} = 0.2 to 0.27, and equivalence ratio ϕ = 0.7 to 1.6. To obtain data less affected by flame non-idealities, the NO measurement point was set at HAB = 5 mm, which is only slightly downstream of the flame

front, thus minimizing the influence of heat loss and species diffusion to/from the environment. The corresponding laminar burning velocity S_L of each flame was also measured using the heat flux method.

Comparison between the present experimental and simulation results indicated that the four models tested, i.e., the Konnov, Glarborg, NOMecha2.0, and San Diego mechanisms cannot reproduce well the NO experimental data for all investigated conditions. By analyzing the measured NO increment at different x_{O_2}, the thermal NO through NO+N = N_2+O (R1) is found to be overpredicted, especially by the Konnov and San Diego mechanisms. From the analyses using the Konnov and Glarborg mechanisms, the increment in NO mole fraction for stoichiometric and fuel-lean flames when x_{O_2} increases is mostly defined by thermal-NO production. The rate constant of reaction NO+N = N_2+O was derived as $k = 1.529 \times 10^{13} T^{-0.0027} \exp(\frac{185.41[cal/mole]}{RT})$ cm^3 / mol s over 225–2400 K range with uncertainty 45% in the negative direction of the pre-exponential factor. The rate constants of four reactions controlling CH mole fraction profiles and prompt-NO formation were updated based on the analysis of the literature data that yields an improved performance of the Konnov mechanism.

Reaction pathway analysis using the updated mechanism indicates that the increase of NO mole fraction at higher x_{O_2} is defined by the increase of the overall reactivity (defined by the chain-branching reaction H + O_2 = OH + O and correlated to S_L) at $\phi = 1.4$, and by the increase of both the rate of production via (R1) and the overall reactivity at $\phi = 1.0$. Thus, through this approach, the thermal-NO reaction channel and its temperature dependence can be better analyzed given that the difference between the contributions from thermal- and prompt NO to the total measured NO mole fraction increases with increasing x_{O_2}.

Declaration of Competing Interest

The authors declare that they have no known competing financial interests or personal relationships that could have appeared to influence the work reported in this paper.

Acknowledgment

This work was supported by the Swedish Energy Agency via the Centre for Combustion Science and Technology (Project KC-CECOST 22538-4), the European Research Council through ERC Advanced Grant TUCLA 669466, the National Scholarship for Building High Level Universities (China Scholarship Council, No. 201906320206) and State Key Laboratory of Clean Energy Utilization (Project ZJUCEU2019001).

Supplementary materials

Supplementary material associated with this article can be found, in the online version, at doi:10.1016/j.combustflame.2020.10.010.

References

[1] P. Glarborg, J.A. Miller, B. Ruscic, S.J. Klippenstein, Modeling nitrogen chemistry in combustion, Prog. Energy Combust. Sci. 67 (2018) 31–68.
[2] A.A. Konnov, Implementation of the NCN pathway of prompt-NO formation in the detailed reaction mechanism, Combust. Flame 156 (2009) 2093–2105.
[3] G.P. Smith, D.M. Golden, M. Frenklach, N.W. Moriarty, B. Eiteneer, M. Goldenberg, C.T. Bowman, R.K. Hanson, S. Song, W. Gardiner Jr., GRI-Mech 3.0, 1999, URL http://www.me.berkeley.edu/gri_mech, (2011).
[4] Chemical-kinetic mechanisms for combustion applications, mechanical and aerospace engineering (combustion research), University of California at San Diego, http://web.eng.ucsd.edu/mae/groups/combustion/mechanism.html, (2014).
[5] N. Lamoureux, H.E. Merhubi, L. Pillier, S. de Persis, P. Desgroux, Modeling of NO formation in low pressure premixed flames, Combust. Flame 163 (2016) 557–575.
[6] K.P. Shrestha, L. Seidel, T. Zeuch, F. Mauss, Kinetic Modeling of NOx formation and consumption during methanol and ethanol oxidation, Combust. Sci. Technol. 191 (2019) 1628–1660.
[7] N. Lamoureux, P. Desgroux, A. El Bakali, J.F. Pauwels, Experimental and numerical study of the role of NCN in prompt-NO formation in low-pressure CH4–O2–N2 and C2H2–O2–N2 flames, Combust. Flame 157 (2010) 1929–1941.
[8] T. Mendiara, P. Glarborg, Ammonia chemistry in oxy-fuel combustion of methane, Combust. Flame 156 (2009) 1937–1949.
[9] C. Brackmann, T. Methling, M. Lubrano Lavadera, G. Capriolo, A.A. Konnov, Experimental and modeling study of nitric oxide formation in premixed methanol + air flames, Combust. Flame 213 (2020) 322–330.
[10] Y. Zhou, Z. Wang, Y. He, R. Whiddon, D. Xu, Z. Li, K. Cen, Effects of CH4 content on NO Formation in one-dimensional adiabatic flames investigated by saturated laser-induced fluorescence and CHEMKIN modeling, Energy Fuels 31 (2017) 3154–3163.
[11] Z. Wang, Y. Zhou, R. Whiddon, Y. He, K. Cen, Z. Li, Investigation of NO formation in premixed adiabatic laminar flames of H2/CO syngas and air by saturated laser-induced fluorescence and kinetic modeling, Combust. Flame 164 (2016) 283–293.
[12] A. Cuoci, A. Frassoldati, A. Stagni, T. Faravelli, E. Ranzi, G. Buzzi-Ferraris, Numerical modeling of NO x formation in turbulent flames using a kinetic post-processing technique, Energy Fuels 27 (2013) 1104–1122.
[13] G.M.G. Watson, P. Versailles, J.M. Bergthorson, NO formation in rich premixed flames of C1–C4 alkanes and alcohols, Proc. Combust. Inst. 36 (2017) 627–635.
[14] S. de Persis, L. Pillier, M. Idir, J. Molet, N. Lamoureux, P. Desgroux, NO formation in high pressure premixed flames: experimental results and validation of a new revised reaction mechanism, Fuel 260 (2020) 116331.
[15] M. Clyne, B.A. Thrush, Kinetics of the reactions of active nitrogen with oxygen and with nitric oxide, Proc. R. Soc. Lond. Ser. A: Math. Phys. Sci. 261 (1961) 259–273.
[16] D. Iverach, K.S. Basden, N.Y. Kirov, Formation of nitric oxide in fuel-lean and fuel-rich flames, Symp. (Int.) Combust. 14 (1973) 767–775.
[17] J.V. Michael, K.P. Lim, Rate constants for the N2O reaction system: thermal decomposition of N2O; N+NO→N2+O; and implications for O+N2→NO+N, J. Chem. Phys. 97 (1992) 3228–3234.
[18] M. Koshi, M. Yoshimura, K. Fukuda, H. Matsui, K. Saito, M. Watanabe, A. Imamura, C. Chen, Reactions of N (4 S) atoms with NO and H2, J. Chem. Phys. 93 (1990) 8703–8708.
[19] P. Heberling, "Prompt NO" measurements at high pressures, Symp. (Int.) Combust. 16 (1977) 159–168.
[20] C. Fenimore, Formation of nitric oxide in premixed hydrocarbon flames, Symp. (Int.) Combust. 13 (1971) 373–380.
[21] F. Kaufman, L. Decker, Effect of oxygen on thermal decomposition of nitric oxide at high temperatures, Symp. (Int.) Combust. 7 (1958) 57–60.
[22] F. Bachmaier, K. Eberius, T. Just, The formation of nitric oxide and the detection of HCN in premixed hydrocarbon-air flames at 1 atmosphere, Combust. Sci. Technol. 7 (1973) 77–84.
[23] R. Atkinson, D. Baulch, R. Cox, R.F. Hampson Jr, J. Kerr, J. Troe, Evaluated kinetic and photochemical data for atmospheric chemistry: supplement III. IUPAC subcommittee on gas kinetic data evaluation for atmospheric chemistry, J. Phys. Chem. Ref. Data 18 (1989) 881–1097.
[24] J. Lee, J. Michael, W. Payne, L. Stief, Absolute rate of the reaction of N (4 S) with NO from 196–400K with DF–RF and FP–RF techniques, J. Chem. Phys. 69 (1978) 3069–3076.
[25] M.A. Clyne, I.S. McDermid, Mass spectrometric determinations of the rates of elementary reactions of NO and of NO 2 with ground state N 4 S atoms, J. Chem. Soc. Faraday Trans. 1: Phys. Chem. Condens. Phases 71 (1975) 2189–2202.
[26] J. Duff, R. Sharma, Quasiclassical trajectory study of the N (4S)+ NO (X2Π)→ N2 (X1Σ+ g)+ O (3P) reaction rate coefficient, Geophys. Res. Lett. 23 (1996) 2777–2780.
[27] D.E. Siskind, D.W. Rusch, Nitric oxide in the middle to upper thermosphere, J. Geophys. Res.: Space Phys. 97 (1992) 3209–3217.
[28] D. Baulch, C.T. Bowman, C. Cobos, R. Cox, T. Just, J. Kerr, M. Pilling, D. Stocker, J. Troe, W. Tsang, Evaluated kinetic data for combustion modeling: supplement II, J. Phys. Chem. Ref. Data 34 (2005) 757–1397.
[29] M. Abian, M.U. Alzueta, P. Glarborg, Formation of NO from N2/O2 mixtures in a flow reactor: toward an accurate prediction of thermal NO, Int. J. Chem. Kinet. 47 (2015) 518–532.
[30] N.A. Buczkó, T. Varga, I.G. Zsély, T. Turányi, Formation of NO in high-temperature N2/O2/H2O mixtures: re-evaluation of rate coefficients, Energy Fuels 32 (2018) 10114–10120.
[31] A.A. Konnov, I.V. Dyakov, J. De Ruyck, Probe sampling measurements and modeling of nitric oxide formation in methane-air flames, Combust. Sci. Technol. 169 (2001) 127–153.
[32] K.J. Bosschaart, M. Versluis, R. Knikker, T.H. Vandermeer, K.R.A.M. Schreel, L.P.H. De Goey, A.A. Van Steenhoven, The heat flux method for producing burner stabilized adiabatic flames: an evaluation with CARS thermometry, Combust. Sci. Technol. 169 (2001) 69–87.
[33] A. Van Maaren, L.P.H. de Goey, Laser doppler thermometry in flat flames, Combust. Sci. Technol. 99 (1994) 105–118.
[34] F.H.V. Coppens, J. De Ruyck, A.A. Konnov, Effects of hydrogen enrichment on adiabatic burning velocity and NO formation in methane+air flames, Exp. Thermal Fluid Sci. 31 (2007) 437–444.

[35] M. Lubrano Lavadera, A.A. Konnov, Data consistency of the burning velocity measurements using the heat flux method: syngas flames, Energy Fuels 34 (2020) 3725–3742.
[36] V.A. Alekseev, J.D. Naucler, M. Christensen, E.J.K. Nilsson, E.N. Volkov, L.P.H. de Goey, A.A. Konnov, Experimental uncertainties of the heat flux method for measuring burning velocities, Combust. Sci. Technol. 188 (2016) 853–894.
[37] CHEMKIN-PRO 17.0 (15151), ANSYS reaction design: San Diego (2016).
[38] G. Capriolo, C. Brackmann, M. Lubrano Lavadera, T. Methling, A.A. Konnov, An experimental and kinetic modelling study on nitric oxide formation in premixed C3 alcohols flames, Proc. Combust. Inst. (2020), doi:10.1016/j.proci.2020.07.051.
[39] H. Nakamura, M. Shindo, Effects of radiation heat loss on laminar premixed ammonia/air flames, Proc. Combust. Inst. 37 (2019) 1741–1748.
[40] D.K. Papanastasiou, J. Bourgalais, T. Gierczak, J.B. Burkholder, N(4S3/2) reaction with NO and NO2: temperature dependent rate coefficients and O(3P) product yield, Chem. Phys. Lett. 728 (2019) 102–108.
[41] P.O. Wennberg, J.G. Anderson, D.K. Weisenstein, Kinetics of reactions of ground state nitrogen atoms (4S3/2) with NO and NO2, J. Geophys. Res.: Atmos. 99 (1994) 18839–18846.
[42] T. Nakayama, K. Takahashi, Y. Matsumi, K. Shibuya, N (4S) formation following the 193.3-nm ArF laser irradiation of NO and NO2 and its application to kinetic studies of N (4S) reactions with NO and NO2, J. Phys. Chem. A 109 (2005) 10897–10902.
[43] J. Burkholder, S. Sander, J. Abbatt, J. Barker, R. Huie, C. Kolb, M. Kurylo, V. Orkin, D. Wilmouth, P. Wine, Chemical kinetics and photochemical data for use in atmospheric studies: evaluation number 18, 2015.
[44] N. Brahms, Generalized nonlinear non-analytic chi-square fitting (https://www.mathworks.com/matlabcentral/fileexchange/9592-generalized-nonlinear-non-analytic-chi-square-fitting), MATLAB Central File Exchange. Retrieved May 3, 2020, 2020.
[45] P. Gamallo, M. González, R. Sayós, Ab initio derived analytical fits of the two lowest triplet potential energy surfaces and theoretical rate constants for the N (4 S)+ NO (X 2 Π) system, J. Chem. Phys. 119 (2003) 2545–2556.
[46] N.E. Meagher, W.R. Anderson, Kinetics of the O (3P)+ N2O reaction. 2. Interpretation and recommended rate coefficients, J. Phys. Chem. A 104 (2000) 6013–6031.
[47] Z. Hong, D. Davidson, E. Barbour, R. Hanson, A new shock tube study of the H+ O2→ OH+ O reaction rate using tunable diode laser absorption of H2O near 2.5μm, Proc. Combust. Inst. 33 (2011) 309–316.
[48] A. Konnov, J. De Ruyck, Temperature-dependent rate constant for the reaction NNH+ O→ NH+ NO, Combust. Flame 125 (2001) 1258–1264.
[49] J.A. Miller, C.T. Bowman, Mechanism and modeling of nitrogen chemistry in combustion, Prog. Energy Combust. Sci. 15 (1989) 287–338.
[50] E. Garcia, P.G. Jambrina, A. Lagana, Kinetics of the H+ CH2→ CH+ H2 reaction at low temperature, J. Phys. Chem. A 123 (2019) 7408–7419.
[51] A. Fomin, T. Zavlev, V.A. Alekseev, I. Rahinov, S. Cheskis, A.A. Konnov, Experimental and modelling study of 1CH2 in premixed very rich methane flames, Combust. Flame 171 (2016) 198–210.
[52] J.M. Hall, E.L. Petersen, An optimized kinetics model for OH chemiluminescence at high temperatures and atmospheric pressures, Int. J. Chem. Kinet. 38 (2006) 714–724.
[53] S.J. Klippenstein, M. Pfeifle, A.W. Jasper, P. Glarborg, Theory and modeling of relevance to prompt-NO formation at high pressure, Combust. Flame 195 (2018) 3–17.
[54] L. Gasnot, P. Desgroux, J. Pauwels, L.J.C. Sochet, Detailed analysis of low-pressure premixed flames of CH4+ O2+ N2: a study of prompt-NO, Combust. Flame 117 (1999) 291–306.
[55] J.W. Thoman, A. McIlroy, Absolute CH radical concentrations in rich low-pressure methane−oxygen−argon flames via cavity ringdown spectroscopy of the A2Δ–X2Π transition, J. Phys. Chem. A 104 (2000) 4953–4961.
[56] P.A. Berg, D.A. Hill, A.R. Noble, G.P. Smith, J.B. Jeffries, D.R. Crosley, Absolute CH concentration measurements in low-pressure methane flames: comparisons with model results, Combust. Flame 121 (2000) 223–235.
[57] P. Versailles, G.M.G. Watson, A.C.A. Lipardi, J.M. Bergthorson, Quantitative CH measurements in atmospheric-pressure, premixed flames of C1–C4 alkanes, Combust. Flame 165 (2016) 109–124.
[58] R. Evertsen, J. Van Oijen, R. Hermanns, L. De Goey, J. Ter Meulen, Measurements of absolute concentrations of CH in a premixed atmospheric flat flame by cavity ring-down spectroscopy, Combust. Flame 132 (2003) 34–42.
[59] A. Bergeat, S. Moisan, R. Méreau, J.-.C. Loison, Kinetics and mechanisms of the reaction of CH with H2O, Chem. Phys. Lett. 480 (2009) 21–25.
[60] R.A. Brownsword, A. Canosa, B.R. Rowe, I.R. Sims, I.W. Smith, D.W. Stewart, A.C. Symonds, D. Travers, Kinetics over a wide range of temperature (13–744K): rate constants for the reactions of CH (ν= 0) with H 2 and D 2 and for the removal of CH (ν= 1) by H 2 and D 2, J. Chem. Phys. 106 (1997) 7662–7677.
[61] K. Becker, R. Kurtenbach, P. Wiesen, Temperature and pressure dependence of the reaction methylidyne radical+ hydrogen, J. Phys. Chem. 95 (1991) 2390–2394.
[62] S. Zabarnick, J. Fleming, M.-.C. Lin, Kinetic study of the reaction CH (X 2Π)+ H2⇄ CH2 (X 3 B 1)+ H in the temperature range 372 to 675K, J. Chem. Phys. 85 (1986) 4373–4376.
[63] A. Bergeat, T. Calvo, F. Caralp, J.-.H. Fillion, G. Dorthe, J.-.C. Loison, Determination of the CH+ O 2 product channels, Faraday Discuss. 119 (2002) 67–77.
[64] M. Röhrig, E.L. Petersen, D.F. Davidson, R.K. Hanson, C.T. Bowman, Measurement of the rate coefficient of the reaction CH+O2 → products in the temperature range 2200 to 2600K, Int. J. Chem. Kinet. 29 (1997) 781–789.
[65] M.W. Markus, P. Roth, T. Just, A shock tube study of the reactions of CH with CO2 and O2, Int. J. Chem. Kinet. 28 (1996) 171–179.
[66] G. Smith, Y. Tao, H. Wang, Foundational fuel chemistry model version 1.0 (FFCM-1), 2016.
[67] C.A. Taatjes, Kinetic isotope effect in the CH [2Π]+ O2 reaction, J. Phys. Chem. 100 (1996) 17840–17845.
[68] F. Keshavarz, S.H. Mousavipour, A single-and multireference study on CH (X2Π) reaction with O2 ($X^3\Sigma^-_g$), Int. J. Chem. Kinet. 51 (2019) 161–177.
[69] N.J. Labbe, R. Sivaramakrishnan, C.F. Goldsmith, Y. Georgievskii, J.A. Miller, S.J. Klippenstein, Weakly bound free radicals in combustion: “Prompt” dissociation of formyl radicals and its effect on laminar flame speeds, J. Phys. Chem. Lett. 7 (2016) 85–89.
[70] S. Carl, M. Van Poppel, J. Peeters, Identification of the CH+ O2→ OH (A)+ CO reaction as the source of OH (A− X) chemiluminescence in C2H2/O/H/O2 atomic flames and determination of its absolute rate constant over the range T= 296 to 511K, J. Phys. Chem. A 107 (2003) 11001–11007.
[71] W.A. Sanders, C.Y. Lin, M.C. Lin, On the importance of the reaction CH2+N2 →HCN+NH as a precursor for prompt NO formation, Combust. Sci. Technol. 51 (1987) 103–108.
[72] V. Vasudevan, R.K. Hanson, C.T. Bowman, D.M. Golden, D.F. Davidson, Shock tube study of the reaction of CH with N2: overall rate and branching ratio, J. Phys. Chem. A 111 (2007) 11818–11830.
[73] N. Lamoureux, C.M. Western, X. Mercier, P. Desgroux, Reinvestigation of the spectroscopy of the A-3Πu–X-3Σg- transition of the NCN radical at high temperature: application to quantitative NCN measurement in flames, Combust. Flame 160 (2013) 755–765.
[74] N. Lamoureux, H. El Merhubi, L. Gasnot, C. Schoemaecker, P. Desgroux, Measurements and modelling of HCN and CN species profiles in laminar CH4/O2/N2 low pressure flames using LIF/CRDS techniques, Proc. Combust. Inst. 35 (2015) 745–752.